TEL AVIV UNIVERSITY

THE IBY AND ALADAR FLEISCHMAN FACULTY OF ENGINEERING

Zandman-Slaner School for Graduate Studies in Engineering

Research proposal toward the degree of "Philosophy Doctor"

Research topic:

Direct numerical simulation of transitions and supercritical regimes in confined three-dimensional flows

הדמייה ממוחשבת של הסתייפויות ומצבים סופר קריטיים בזרימות תלת-ממדיות בנפחים סגורים.

Submitted by

Yuri Feldman

Department of Fluid Mechanics and Heat transfer

B.Sc: Mechanical Engineering, Faculty of Mechanical Engineering, Technion, Haifa 2001.

M.Sc: Mechanical Engineering, Faculty of Mechanical Engineering, Technion, Haifa 2006.

Approval of the Supervisors:

I agree to guide the student **Yuri Feldman** in his research work toward the degree of Ph.D and approve his research proposal.

Supervisors Name: **Prof. Alexander Gelfgat,** Signature:----------.

May 2008

אייר תשס"ט-מאי 2008

1. Introduction

The objective of the proposed research is twofold. At the first stage we intend to develop an efficient three-dimensional time marching solver yielding reliable DNS (direct numerical simulation) results for confined three-dimensional flows in flow regions with realistic physical boundary conditions. The term "realistic boundary conditions" assume those conditions that can be realized experimentally, e.g., no-slip conditions. An example of "unrealistic conditions" in this sense is conditions of translational symmetry. The numerical solution must be obtained with a reliable accuracy, which means use of fine grids. We had set effective computations using a non-uniform grid of 100^3 nodes as a primary target. For test calculations we consider two well-known model flows in a three-dimensional rectangular box: a natural convection flow and a three-dimensional lid-driven cavity flow. Two-dimensional versions of these problems are used for benchmarking purposes only. At the second stage of the research a series of DNS computations will be carried out with the purpose to study supercritical oscillatory flow regimes. To complete this task it will be necessary to gather a large amount of numerical data, sufficient for its statistical post-processing. We estimate that we'll need several tens of thousands time steps corresponding to analyze a single asymptotically stable unsteady regime. Therefore we are searching for a numerical method yielding the least CPU-time consuming time integration. Having in mind future applications of this method to applied problems of materials processing we do not want our numerical method to be restricted by a certain type of boundary conditions or shape of flow domain. We are willing also to check a possibility of transformation of our three-dimensional time-stepper into a fully three-dimensional stability solver.

Time marching solver: we discuss a possible acceleration of 2D and 3D time marching algorithms by implementation of a direct linear sparse matrices solver to the time-propagation operator itself, or a similar semi-analytical approach to the inner iteration of a multigrid iteration procedure. Both approaches do not need the pressure-velocity decoupling, which is already an advantage [1]. In the first case the solution is based on an *LU* factorization of the Stokes operator, defined on the whole computational domain. The *LU* factorization is carried out by a direct multifrontal sparse solver (we use the MUMPS package) and is performed only once at the beginning of the time-stepping procedure. The successive calculation of the velocity and pressure fields is obtained by the backward substitution procedure also realized for sparse triangular *L* and *U* matrices.

Another approach utilizes the block implicit multigrid solution based on a coupled line Gauss-Seidel smoother (CLGS) [2]. The line-wise smoother computes pressure and velocity corrections simultaneously over the entire row of finite volumes. We had derived an analytical solution of this assembled equations system, which drastically accelerated the whole iterative process. The modified method is extremely fast since it needs no more than O(5*N*) operations to compute the values of *N* corrections over the entire row for both 2D and 3D geometries. A typical *V-cycle* technique [3] is used for multigrid solution of the problem.

Natural convection flow: natural convection is produced by non-uniform density distribution resulted by the fluid temperature deviation. The phenomenon is of considerable scientific and engineering importance relating to the problems of crystal growth, solar energy collectors, electronic equipment cooling, thermal comfort in buildings and compartment fires. It has been extensively studied inside rectangular two- and three-dimensional cavities because of geometrical simplicity of the boundary conditions. Most of them can be classified in three main groups: cavities where the flow is due to internal heat generation, cavities heated from below (Rayleigh-Bernard configuration), and those heated or cooled from their sides. The configuration of the latter class named also differentially heated cavity is an objective of the present research.

Lid-driven cavity flow: the motion of a Newtonian fluid within a lid-driven rectangular three-dimensional cavity is maintained by the continuous momentum diffusion from the moving wall. Large pressure gradients existing close to the cavity non-slip boundaries, lead to three-dimensional flow phenomenon. Therefore, despite its simple geometry, the lid-driven cavity flow exhibits features of more complex geometry flows, comprising one of the most important benchmarks for numerical Navier-Stokes (NS) solvers.

2. Scientific Background

Natural convection in enclosures, as well as lid-driven cavity flow are traditional benchmark problems widely used in computational fluid mechanics. Having simple geometry and boundary conditions both configurations allow us to examine ability of different CFD methods to predict features of complex flows governed by NS and energy equations.

An extensive literature survey reveals a large number of papers devoted to natural convection and lid-driven cavity flows. Here we review only those that are directly relevant to the present study.

2.1 Free convection in a differentially heated cavity

2.1.1 Steady state flows

Steady state flows in a two dimensional thermally-driven cavity have been used to validate numerical models during last three decades. The main benchmark case proposed by G. de Vahl Davis [4] corresponds to the air convection with Prandtl number of 0.71. Benchmark-quality steady state solutions for the Rayleigh numbers of 10^3,10^4,$10^5$and 10^6 and adiabatic horizontal walls were obtained by Le Quere and Alziary de Roquefort [5]. These results are in good agreement with those obtained in later studies [6-8] that applied stretching at the near-wall regions to resolve very thin boundary layers developing at large Rayleigh numbers of 10^6 and more. Along with two-dimensional studies continuing also nowadays, convection in three-dimensional differentially heated cavity had being explored. Pioneering three-dimensional studies were performed on rather coarse grids and intended to obtain qualitative visualization of the flow rather then its quantitative characteristics (see e.g. [9,10]). Further 3D studies [11-14] focused on revealing of similarities and discrepancies between two- and three-dimensional flows. It was shown that the flow exhibits clear three-dimensional properties close to non-slip boundaries. In more recent studies the steady state

solutions for values of Rayleigh number varying between 10^4 and 10^7 on 111^3 grid [15] and 120^3 grid [16] were calculated. The results reported in [16] were obtained for a high grid resolution and fourth order finite-differences scheme are therefore are believed to be rather accurate. Therefore they are used as a reference for the validation of the numerical code developed in the present study.

2.1.2 Transition to unsteadiness and unsteady flows

Despite a clear three-dimensional physics of the phenomena the prohibitive computational costs of the three-dimensional numerical simulations restricted the majority of previous studies on steady states, transition and supercritical natural convection flows in enclosed cavities to two dimensional formulations.

The configuration with perfectly conducting horizontal walls is more unstable than the configuration with adiabatic ones due to the presence of high temperature areas at the bottom of the cavity. The transition to unsteadiness in a square cavity with conducting horizontal walls was studied by Winters [17] who obtained a critical number $Ra_{cr}=2.109\times10^6$. Later it was confirmed by Jones and Briggs [18] performing three-dimensional experiments and two-dimensional numerical simulations. For the square cavity with adiabatic horizontal walls, the critical Rayleigh number is close to 1.82×10^8 [19], which is almost two orders of magnitude larger than that for conducting boundaries. Le Quere [20] studied convection in a cavity with adiabatic horizontal walls and height to length aspect ratio equal to 4 and found a primary Hopf bifurcation at $Ra_{cr}=1.03\times10^8$. He observed also a chaotic behavior beyond $Ra=2.3\times10^8$. An extensive two-dimensional unsteady analysis for differentially heated cavity with height to length aspect ratio 8 was performed by Xin and Le Quere [21]. It was found that beyond a critical Rayleigh number, the flow becomes time dependent (periodic, chaotic and eventually fully turbulent). This problem was also defined as a benchmark case with the main bulk of results summarized in [22]. For this configuration, the critical Rayleigh number is $Ra_{cr}=3.0619\times10^5$. In addition, a valuable experimental [2324] and numerical [25] data was obtained investigating supercritical flows in two-dimensional square and three-dimensional tall cavities, respectively.

The transition from quasi-two-dimensional steady laminar to a three-dimensional time-dependent regime was first considered in [26] for the case of perfectly conducting horizontal walls in a cubic cavity with solid vertical walls and numerically imposing flow symmetries. The study was then extended to the configuration of differentially heated cubic cavity for the case of adiabatic horizontal walls [27]. It was found that the critical Rayleigh numbers for the transition to unsteadiness are between $2.25\div2.35\times10^6$ and between $2.5\div 3\times10^8$ for configurations with perfectly conducting and adiabatic horizontal walls, respectively, which is larger than those of the two-dimensional configurations. Only several unsteady studies have been performed regarding realistic boundary conditions, without assuming symmetry or periodicity. Fusegi et al. [28] investigated an oscillatory flow regime for the case of perfectly conducting walls in a cubic cavity for $Ra=8.5\times10^6$. Labrosse et al. [29] extended this study for the configuration with adiabatic horizontal walls and found a non-symmetric transition for $Ra= 3.19\times10^7$, which is significantly lower than in the similar two-dimensional case. A number of DNS was performed to obtain a time-averaged quantities and

statistics of the supercritical flows [30,31]. However, three-dimensional structure of confined convective flows is far from being fully understood. Many differences between numerical and experimental results remain unexplained. For example, thermal stratification in the cavity still cannot be predicted well [25]. Moreover, the existing DNS results [30,33] needed to be improved since they are restricted to periodical boundary conditions in second horizontal direction and are performed on a too coarse grids with less than 100 nodes in the shortest direction, which according to Gelfgat [34] would not provide the quantitatively correct results.

2.2 Lid-driven cavity flow

2.2.1 Steady state flows

The steady state lid-driven cavity flow is considered as a classical test problem for the assessment of numerical methods and validation of NS codes. Ghia et al. [35] and Schreiber and Keller [36] were among the first to report benchmark data on the lid-driven cavity flow. At about the same time, the interest in the flow physics of confined recirculating flows was revived after the pioneering works of Burgraf [37] and Pan and Acrivos [38]. The renewed interest led to a series of papers focusing on three-dimensional vertical structures and on end-wall effects, see e.g. [39,40]. Over the years the grid resolution and the numerical accuracy were significantly improved and even more accurate solutions of the two-dimensional problem have been obtained using spectral methods [41,42].

Three-dimensional properties of the lid-driven cavity flow have been firstly studied by Davis and Mallinson [43] and Goda [44]. The relevance of three-dimensional flows in general was demonstrated by Freitas et al [45]. In particular, three-dimensional effects near the end-walls of a finite-size system, which always exist in a laboratory setup, were emphasized in [46]. During last years, further three-dimensional steady state calculations have been performed, e.g., in [47-50]. Studies of [51-54] primarily focused on the flow structure topology and not on benchmarking. Recently an accurate three-dimensional benchmark solution was obtained by Albensoeder and Kuhlmann [55] who treated a steady state flow at $Re=10^3$ by a Chebyshev-collocation method, providing a high spatial accuracy of the results. These results are used here as a reference for validation of the present numerical model.

2.2.2 Transition to unsteadiness and unsteady flows

Since two-dimensional, time-dependent calculations are significantly less costly than full three-dimensional simulations, the Hopf bifurcation at high Reynolds numbers of purely two-dimensional flow was extensively investigated with a rather good precision [56-60]. Being important for benchmarking these resluts cannot describe completely realistic 3D flows. The oscillatory two-dimensional flows exist for such high Reynolds numbers $Re=O(10^4)$ that they are very unlikely to be observed experimentally. Albensoeder et al. [61] showed that quasi-two-dimensional steady flow becomes unstable to genuinely three-dimensional flows at Reynolds number one order of magnitude smaller than those at which the two-dimensional flow oscillations have been computed. In order to clarify the observed three-dimensional flow structures numerically

a series of benchmark tests for the lid-driven cavity was undertaken for a Reynolds number of 3200. The results, however, remained inconclusive, since the numerical simulations obtained by different methods and resolutions exhibited a significant disagreement [62].

After becoming unsteady, with further increase of the Reynolds number the three-dimensional cavity flow develops into a turbulent regime. Surprisingly, there is almost no numerical results for Reynolds numbers of the order of $Re=O(10^4)$ and larger except DNS study by Leiriche and Gavrilakis [63] and LES (Large Eddy Simulation) simulation by Bouffanias et al. [64].

The foregoing survey revealed a severe lack of numerical data describing the three-dimensional flow transitions to unsteadiness and hydrodynamic features of supercritical flows regarding thermally- and lid-driven cavities. Taking into account the physical and technological significance of laminar three-dimensional supercritical flows and continuous growth of computational recourses a systematic study of three-dimensional supercritical flows should be performed. The main guidelines and purposes of the present research are detailed in the next section.

3. Research Objectives and Significance

The aim of the present research is to perform systematic study of three-dimensional steady and supercritical flows developing in differentially heated or lid-driven rectangular three-dimensional boxes. For each configuration no-slip boundary conditions are applied in all the spatial directions. The main goal is to to determine important topology characteristics of three-dimensional steady and unsteady flows in configurations that can be realized in a laboratory experiment. The numerical simulations performed with high temporal and spatial resolutions, (no less the 100 nodes in the shortest direction as was stated in [34]) providing full-scale spectrum of the frequencies and eddies characterizing the specific flow. The performed research would extend our understanding of the flow pattern spatio-temporal evolution at large Grashof and Reynolds numbers. The study includes:

i. Development of a robust numerical tool for solving unsteady three-dimensional NS and energy equations. An extensive validation study should be performed by a comparison of obtained results with existing benchmark solutions. Particular emphasis should be placed on numerical robustness augmenting of the developed algorithm by utilizing the semi-implicit temporal discretization of convective terms. This would allow to enlarge the time step and to provide a necessary amount of numerical data needed for forthcoming statistical post-processing. Last but not least, the numerical simulations should be accelerated by the code parallelization taking advantage of available modern, massively parallel supercomputers.
ii. Direct numerical simulation will be carried out for thermally- and lid-driven cavities. Both transient and periodical states of the flow posses long time scales requiring long integration times (no less then several hundred periods in the case of a periodic flow). The critical Reynolds and Grashof numbers corresponding to the first Hopf bifurcation point for steady-periodical transition would be obtained, which will be followed by an attempt to localize consequent bifurcations. Given the detailed full-scale numerical data would provide the basis

for considering the scaling behavior of the mean temperature, the mean velocity profile and of the profiles of different turbulence statistics.

iii. The post-processing of supercritical oscillatory regimes should be performed in terms of statistical turbulence parameters: mean values of the primitive variables (velocity components, pressure and temperature), Reynolds stresses, velocity correlations, turbulence intensity, and turbulence kinetic energy. Such statistic analysis would shed light on spatial topology of supercritical flows, determining the dominant flow scales and hydrodynamic mechanisms responsible for the flow redistribution inside the cavities. A large enough amount of the time-dependent data will allow also for calculations of such stochastic properties as Lyapunov exponents and fractal dimensions.

iv. As an option a problem of stability of steady convective and lid-driven flows may be studied. The onset of oscillatory instability for the flow in differentially heated and lid-driven cavities will be located by computing a steady-state and analyzing its stability via an eigenvalue problem. The analysis would reveal the characteristics and the manner of mutual influence of dominant modes determining the system physics. The stability analysis implies development of an effective three-dimensional steady state solver, which would be based on the Newton-Raphson method owing to non-linear character of the NS equations.

4. Methodology and Research plan

4.1 Formulation of the problem.

4.1.1 Differentially heated cavity – governing equations.

Natural convection in a three dimensional box of length *W*, height *H* and width *D* is considered (see Fig. 1). The box aspect ratio is *A=H/W* and the width ratio is *B*=D/W. Two opposite vertical walls of the box are maintained at different constant temperatures whereas all four remaining walls are either adiabatic or perfectly conducting.

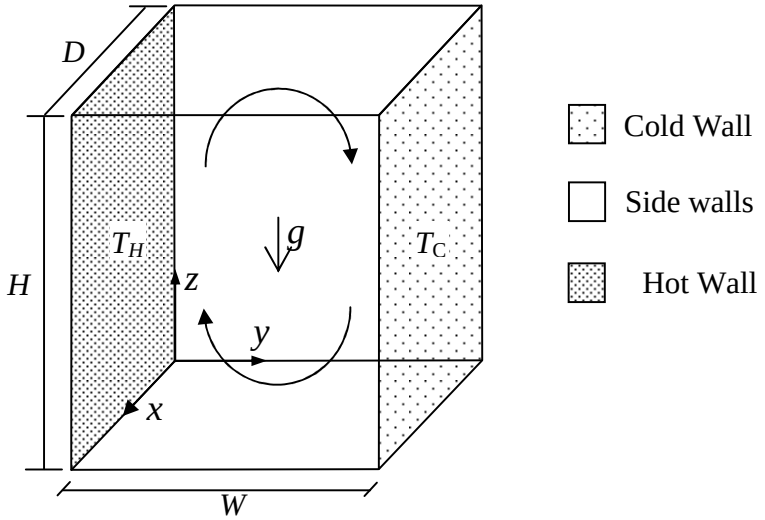

Figure 1. Differentially heated cavity -physical model and coordinate system.

The flow is described by the momentum, energy and continuity equations in the Boussinesq approximation. Following Ref. [21], the dimensionless governing equations are:

$$\nabla \cdot \boldsymbol{u} = 0 \tag{1}$$

$$\frac{\partial \boldsymbol{u}}{\partial t} + (\boldsymbol{u} \cdot \nabla)\boldsymbol{u} = -\nabla p + \frac{1}{\mathrm{Gr}^{0.5}} \nabla^2 \boldsymbol{u} + \theta \overrightarrow{e_z} \tag{2}$$

$$\frac{\partial \theta}{\partial t} + (\boldsymbol{u} \cdot \nabla)\theta = \frac{1}{\mathrm{Pr}\,\mathrm{Gr}^{0.5}} \nabla^2 \theta \tag{3}$$

where $\boldsymbol{u}=(u,v,w)$, p, t, and θ are the dimensionless velocity, pressure, time and temperature, respectively, and $\vec{e}_z$ is the unit vector in the z direction. These non-dimensional equations were obtained using characteristic length W (see Fig.1), buoyancy velocity scale $U = \sqrt{g\beta W \Delta T}$, time scale $t = W/U$, and pressure scale $P = \rho U^2$. Here ρ is the mass density, g is the gravitational acceleration, β is the isobaric coefficient of thermal expansion, and $\Delta T = T_H - T_C$ is the temperature difference between the hot and cold walls. The dimensionless temperature θ is defined in terms of the wall temperature difference as:

$$\theta = (T - T_C)/\Delta T \tag{4}$$

The Grashof number is

$$\mathrm{Gr} = \frac{g\beta \Delta T W^3}{\nu^2} \tag{5}$$

and the Prandtl number is

$$\mathrm{Pr} = \nu/\alpha \tag{6}$$

where ν is the kinematic viscosity, and α is the thermal diffusivity.

4.1.2 Lid-driven cavity -governing equations.

Lid driven flow inside a box of length W, height H and width D is considered (see Fig. 2). Similarly to the previous model the cavity is characterized by aspect and width ratios defined as $A=H/W$ and $B=D/W$, respectively. The top wall of the cavity is moving in y direction with a constant velocity v, while all other cavity walls are stationary. No external body forces are acting.

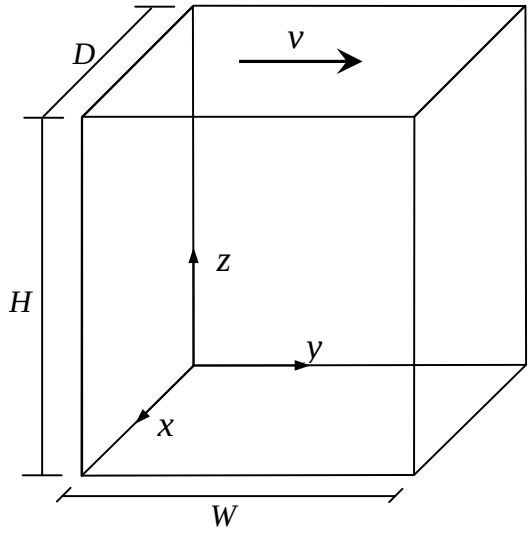

Figure 2. Lid-driven cavity - physical model and coordinate system.

The flow is described by the momentum and continuity equations. The dimensionless governing equations are:

$$\nabla \cdot \boldsymbol{u} = 0 \tag{7}$$

$$\frac{\partial \boldsymbol{u}}{\partial t} + (\boldsymbol{u} \cdot \nabla)\boldsymbol{u} = -\nabla p + \mathrm{Re}^{-1} \nabla^2 \boldsymbol{u} \tag{8}$$

where $\boldsymbol{u}=(u,v,w)$, t and p are the dimensionless velocity, time and pressure respectively. The dimensionless equations were obtained utilizing the characteristic length W (see Fig.2), velocity scale $U = v$ and scales for time and pressure similar to those chosen for the differentially heated cavity.

4.2. Discretization in time and space.

The time derivative in the unsteady momentum and the energy equations is approximated by a second order backward differentiation formula:

$$\frac{\partial f^{n+1}}{\partial t} = \frac{3f^{n+1} - 4f^{n} + f^{n-1}}{2\Delta t} + O(\Delta t^2) \tag{9}$$

In both models diffusion terms are treated implicitly while convective terms are treated explicitly. In the free convection problem, rearranging of all explicit terms to the right hand side (*RHS*) allows one to decouple the energy equation (3) from the continuity and momentum equations (1) and (2) and to present the momentum equation (2) in the form defined by the Stokes operator. The momentum equation (8) in the lid-driven cavity problem is treated in the same way. Due to the explicit advancement of the nonlinear terms, the overall scheme is subjected to restrictions in the size of the time step. Thus the time increment must satisfy the usual Courant number criterion for purely explicit schemes:

$$C_x = |u|\Delta t / \Delta x < 1.0, C_y = |v|\Delta t / \Delta y < 1.0, C_z = |w|\Delta t / \Delta y < 1.0 \tag{10}$$

Also, when a non-zero value of kinematic viscosity and thermal diffusivity are used, momentum and thermal energy must not diffuse more than one cell in one time step, leading to:

$$(\nu, \alpha)\Delta t\left[1/(\Delta x)^2 + 1/(\Delta y)^2 + 1/(\Delta z)^2\right] \le \frac{1}{2} \tag{11}$$

Through the number of numerical tests it was found that for discretization having no less than 100 nodes in the shortest direction the time steps of $\Delta t = 1\times10^{-2}$ and $\Delta t = 4\times10^{-3}$ convergence to steady states insensitively to initial conditions for regular and stretched grids, respectively.

4.2.1 Differentially heated cavity –the numerical procedure.

Calculations in this case proceed as follows.

1. Assume initial pressure and velocity distributions and solve the energy Eq. (3):

$$\frac{1}{\mathrm{Pr}\,\mathrm{Gr}^{0.5}}\nabla^2\theta^{(n+1)} - \frac{3}{2\Delta t}\theta^{(n+1)} = \left[(\boldsymbol{u}\cdot\nabla)\theta\right]^n + \frac{1}{2\Delta t}\left(-4\theta^n + \theta^{(n-1)}\right) \tag{12}$$

2. Substitute the obtained temperature into the momentum equations and solve the coupled continuity - momentum Eqs. (1) – (2):

$$\nabla \cdot \boldsymbol{u}^{(n+1)} = 0 \tag{13}$$

$$\frac{1}{\mathrm{Gr}^{0.5}}\nabla^2\boldsymbol{u}^{(n+1)} - \frac{3}{2\Delta\tau}\boldsymbol{u}^{(n+1)} - \nabla p^{(n+1)} = \left[(\boldsymbol{u}\cdot\nabla)\boldsymbol{u}\right]^n + \frac{1}{2\Delta t}\left(-4\boldsymbol{u}^n + \boldsymbol{u}^{(n-1)}\right) - \theta^{(n+1)}\vec{e}_z \tag{14}$$

A conservative second order accuracy finite volume method [65] is used for the spatial discretization of the Eqs. 12-14). A staggered mesh (see Fig.3) has been used to eliminate the possibility of checkerboard volumes of pressure and velocity fields [65].

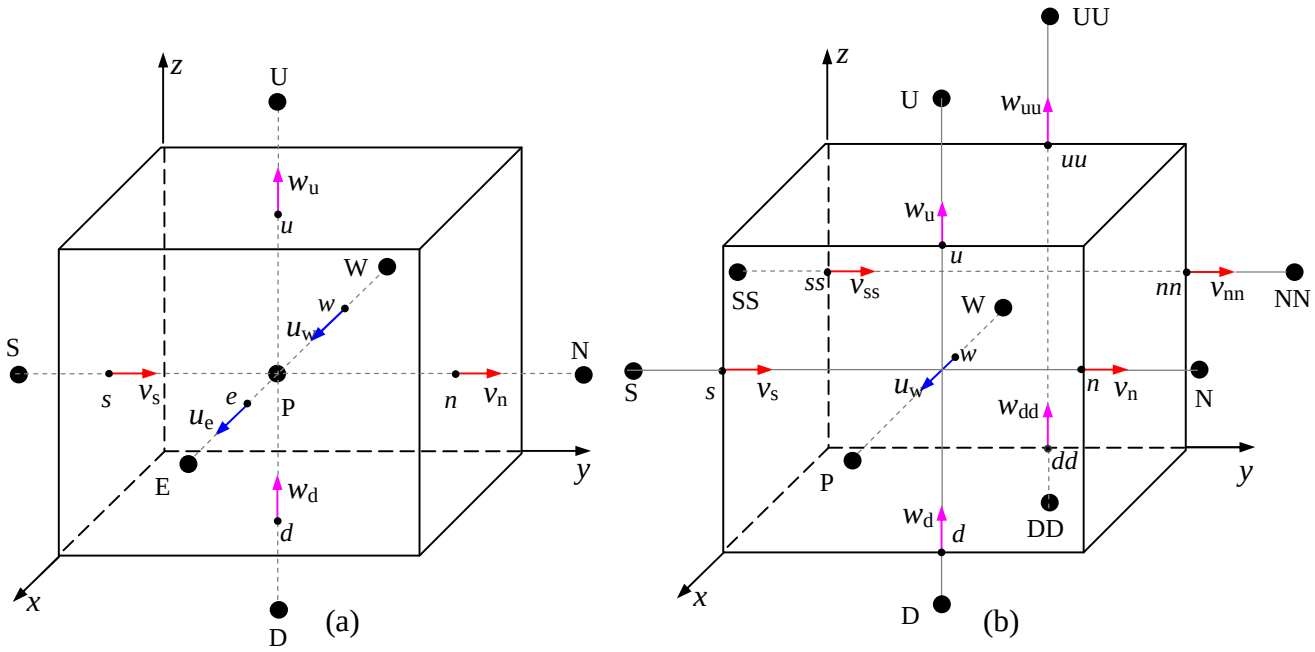

Fig.3 Staggered grid arrangement (a) control volume for scalar fields, (b) control volume for u velocity component.

Note that the control volumes for *v* and *w* velocity components are directly obtained by a 90° rotation of the *u* component control volume (see Fig. 3-b) around the *z* and the *y* axis, respectively.

Utilizing the staggered grid arrangement (see Fig.3), we derive finite volume discretization of Eqs. (12-14) :

$$\left(\frac{1}{\mathrm{P\,r\,Gr}^{0.5}}a_{\mathrm{P}}^{\theta}-\frac{3}{2\Delta t}\right)\theta_{\mathrm{P}}^{\mathrm{n+1}}+\frac{1}{\mathrm{P\,r\,Gr}^{0.5}}\sum_{\mathrm{nb}}a_{\mathrm{nb}}^{\theta}\theta_{\mathrm{nb}}^{\mathrm{n+1}}=RHP_{\theta}^{\mathrm{n}} \tag{15}$$

$$\left(u_{\mathrm{e}}^{\mathrm{n+1}}-u_{\mathrm{w}}^{\mathrm{n+1}}\right)/\left(x_{\mathrm{e}}-x_{\mathrm{w}}\right)+\left(v_{\mathrm{n}}^{\mathrm{n+1}}-v_{\mathrm{s}}^{\mathrm{n+1}}\right)/\left(y_{\mathrm{n}}-y_{\mathrm{s}}\right)+\left(w_{\mathrm{u}}^{\mathrm{n+1}}-w_{\mathrm{d}}^{\mathrm{n+1}}\right)/\left(z_{\mathrm{u}}-z_{\mathrm{d}}\right)=0 \tag{16}$$

$$\left(\frac{1}{\mathrm{Gr}^{0.5}}a_{\mathrm{e}}^{\mathrm{u}}-\frac{3}{2\Delta t}\right)u_{\mathrm{e}}^{\mathrm{n+1}}+\frac{1}{\mathrm{Gr}^{0.5}}\sum_{\mathrm{nb}}a_{\mathrm{nb}}^{\mathrm{u}}u_{\mathrm{nb}}^{\mathrm{n+1}}-\frac{p_E^{n+1}-p_P^{n+1}}{x_E-x_P}=RHP_{\mathrm{u}}^{\mathrm{n}} \tag{17.1}$$

$$\left(\frac{1}{\mathrm{Gr}^{0.5}}a_{\mathrm{n}}^{\mathrm{v}}-\frac{3}{2\Delta t}\right)v_{\mathrm{n}}^{\mathrm{n+1}}+\frac{1}{\mathrm{Gr}^{0.5}}\sum_{\mathrm{nb}}a_{\mathrm{nb}}^{\mathrm{v}}v_{\mathrm{nb}}^{\mathrm{n+1}}-\frac{p_N^{n+1}-p_P^{n+1}}{y_N-y_P}=RHP_{\mathrm{v}}^{\mathrm{n}} \tag{17.2}$$

$$\left(\frac{1}{\mathrm{Gr}^{0.5}}a_{\mathrm{d}}^{\mathrm{u}}-\frac{3}{2\Delta t}\right)w_{\mathrm{u}}^{\mathrm{n+1}}+\frac{1}{\mathrm{Gr}^{0.5}}\sum_{\mathrm{nb}}a_{\mathrm{nb}}^{\mathrm{v}}w_{\mathrm{nb}}^{\mathrm{n+1}}-\frac{p_U^{n+1}-p_P^{n+1}}{z_U-z_P}=RHP_{\mathrm{w}}^{\mathrm{n}} \tag{17.3}$$

Expressions for the coefficients a_{p}, a_{e}, a_{n}, a_{d}, a_{nb} for each unknown function are obtained by the finite volume discretization of the Laplace operator. Expressions for $RHP_{\theta}^{\mathrm{n}}$, $RHP_{\mathrm{u}}^{\mathrm{n}}$, $RHP_{\mathrm{v}}^{\mathrm{n}}$, $RHP_{\mathrm{w}}^{\mathrm{n}}$ consist of time discretization terms of the functions and finite volume representation of

convective terms known from previous time step (see **Appendix A**[70] for the discretization details).

4.2.2 Lid-driven cavity -numerical procedure.

The discretization of continuity and momentum equations (7-8) is performed in the same way as for the differentially heated cavity:

$$\left(u_{\mathrm{e}}^{\mathrm{n}+1}-u_{\mathrm{w}}^{\mathrm{n}+1}\right)/\left(x_{\mathrm{e}}-x_{\mathrm{w}}\right)+\left(v_{\mathrm{n}}^{\mathrm{n}+1}-v_{\mathrm{s}}^{\mathrm{n}+1}\right)/\left(y_{\mathrm{n}}-y_{\mathrm{s}}\right)+\left(w_{\mathrm{u}}^{\mathrm{n}+1}-w_{\mathrm{d}}^{\mathrm{n}+1}\right)/\left(z_{\mathrm{u}}-z_{\mathrm{d}}\right)=0 \qquad (18)$$

$$\left(\mathrm{Re}^{-1}a_{\mathrm{e}}^{\mathrm{u}}-\frac{3}{2\Delta t}\right)u_{\mathrm{e}}^{\mathrm{n}+1}+\mathrm{Re}^{-1}\sum_{\mathrm{nb}}a_{\mathrm{nb}}^{\mathrm{u}}u_{\mathrm{nb}}^{\mathrm{n}+1}-\frac{p_E^{n+1}-p_P^{n+1}}{x_E-x_P}=RHP_{\mathrm{u}}^{\mathrm{n}} \qquad (19.1)$$

$$\left(\mathrm{Re}^{-1}a_{\mathrm{n}}^{\mathrm{v}}-\frac{3}{2\Delta t}\right)v_{\mathrm{n}}^{\mathrm{n}+1}+\mathrm{Re}^{-1}\sum_{\mathrm{nb}}a_{\mathrm{nb}}^{\mathrm{v}}v_{\mathrm{nb}}^{\mathrm{n}+1}-\frac{p_N^{n+1}-p_P^{n+1}}{y_N-y_P}=RHP_{\mathrm{v}}^{\mathrm{n}} \qquad (19.2)$$

$$\left(\mathrm{Re}^{-1}a_{\mathrm{d}}^{\mathrm{u}}-\frac{3}{2\Delta t}\right)w_{\mathrm{u}}^{\mathrm{n}+1}+\mathrm{Re}^{-1}\sum_{\mathrm{nb}}a_{\mathrm{nb}}^{\mathrm{v}}w_{\mathrm{nb}}^{\mathrm{n}+1}-\frac{p_U^{n+1}-p_P^{n+1}}{z_U-z_P}=RHP_{\mathrm{w}}^{\mathrm{n}} \qquad (19.3)$$

where the expressions for the all coefficients and *RHS* parts are derived by the same finite volume discretization as for differentially heated cavity (see **Appendix A**[70] for the discretization details) . As for the previous model the discretized equations (18) and (19.1)-(19.3) are solved with a complete coupling of pressure and velocity.

4.2 Solution algorithms

4.2.1The Full Pressure Coupled Direct (FPCD) Solution.

The algorithm is based on an *LU* factorization of the Stokes operator, defined on the whole computational domain. The *LU* factorization is carried out by a direct multifrontal sparse solver (we use the MUMPS package) and is performed only once at the beginning of the time-stepping procedure. The successive calculation of the velocity and pressure fields is obtained by the backward substitution procedure also realized for sparse triangular *L* and *U* matrices. Due to effective utilization of the matrix sparsity both *LU*- factorization and back substitution are relatively fast. The characteristic CPU times and memory requirements needed for the *LU*-factorization are detailed in [34]. The flow chart of the algorithm is detailed in **Appendix B**[70].

The boundary conditions are of the Dirichlet type for velocities (no slip boundary condition), the Dirichlet and the Newman type for temperatures (perfectly conducting or adiabatic walls respectively). No pressure boundary conditions are needed because eqs. (19.1)-(19.3) include pressure values in inner nodes only. The resulting system is singular since the pressure is defined within an addition of a constant. The singularity is removed by adding a Dirichlet point at the corner node. For free convection flow inside the differentially heated cavity the decoupled energy equation (3) was solved by the Bi-CGSTAB algorithm [66]. By this way we decrease a computer memory usage up to about 20 percent comparing with solving the same equation by the MUMPS package. It was also found that for the energy equation the Bi-CGSTAB and the MUMPS consume almost same CPU time.

4.2.2 The Multigrid Solution.

The developed algorithm is a modification of the method originally developed and validated by Vanka for a square [67] and cubic [68] lid-driving cavities. Linearity of the Stokes operator allows us to use the correction scheme (CS) of Ref. [69] and the Coupled Line Gauss-Seidel smoother (CLGS) developed in [2]. A typical *V-cycle* technique [3] is used for the multigrid iterations. A flowchart and detailed explanations can be found in **Appendix C [**70]. Contrary to so called *self-controlling* algorithms detailed in [67,68] the *V-cycle* technique is controlled only by the rate of convergence and does not require any additional accommodative criteria for switching from one grid to another [69]. Therefore it is expected to be more efficient for analysis of unsteady flows proceeding with small time intervals and characterized by small flow variations between two sequential time steps. The line-wise smoother computes the pressure and the velocity corrections simultaneously over the entire row of finite volumes. We derived an analytical solution of this assembled equations system. The modified method, based on Accelerated Semi-Analytic Coupled Line Gauss-Seidel smoother (ASA-CLGS) is extremely fast since it needs no more than O(5*N*) operations to compute the values of *N* corrections over the entire row for both 2D and 3D geometries. The overall complexity of the algorithm however is larger and strongly depends on a discretization method, as a result of additional computations involved in updating *RHS* parts after obtaining the corrections over each row. The characteristic CPU times consumed for a single time step per one node and per one CPU for both approaches are of order 5×10^{-3} msec and 10^{-2} msec for 2D and 3D calculations, respectively.

4.2.2.1 The ASA-CLGS smoother details

We start the description from the characteristic matrix for the coupled pressure-velocity corrections for the SCGS smoother developed in [67]. This matrix is illustrated in Fig.4.

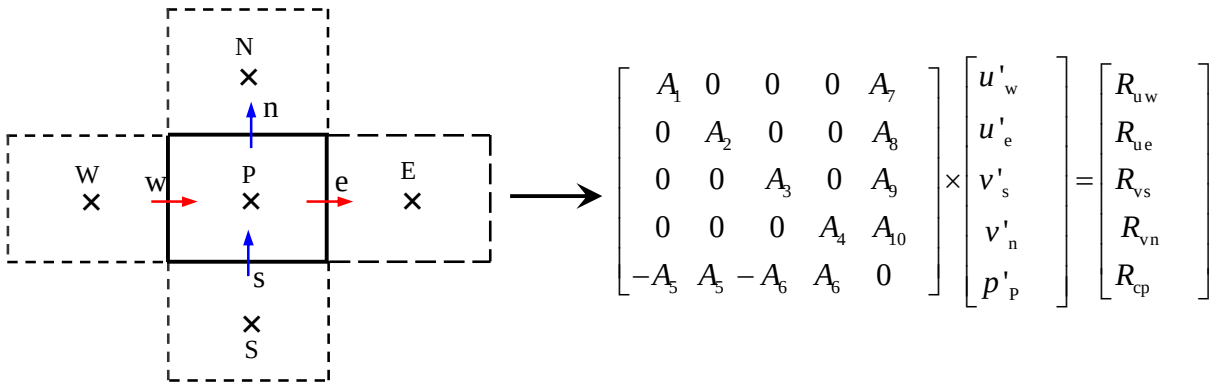

$$\begin{bmatrix} A_1 & 0 & 0 & 0 & A_7 \\ 0 & A_2 & 0 & 0 & A_8 \\ 0 & 0 & A_3 & 0 & A_9 \\ 0 & 0 & 0 & A_4 & A_{10} \\ -A_5 & A_5 & -A_6 & A_6 & 0 \end{bmatrix} \times \begin{bmatrix} u'_{\mathrm{w}} \\ u'_{\mathrm{e}} \\ v'_{\mathrm{s}} \\ v'_{\mathrm{n}} \\ p'_{\mathrm{P}} \end{bmatrix} = \begin{bmatrix} R_{\mathrm{uw}} \\ R_{\mathrm{ue}} \\ R_{\mathrm{vs}} \\ R_{\mathrm{vn}} \\ R_{\mathrm{cp}} \end{bmatrix}$$

Fig.4 Single finite volume matrix for Symmetrical Coupled Gauss-Seidel (SCGS) smoother [67].

For free convection problem defined by discretized equations (12-14) we have $A_1 = \frac{1}{\mathrm{Gr}^{0.5}} a_{\mathrm{w}}^{\mathrm{u}} - \frac{3}{2\Delta t}$,

$A_2 = \frac{1}{\mathrm{Gr}^{0.5}} a_{\mathrm{e}}^{\mathrm{u}} - \frac{3}{2\Delta t}$, $A_3 = \frac{1}{\mathrm{Gr}^{0.5}} a_{\mathrm{w}}^{\mathrm{u}} - \frac{3}{2\Delta t}$, $A_4 = \frac{1}{\mathrm{Gr}^{0.5}} a_{\mathrm{n}}^{\mathrm{v}} - \frac{3}{2\Delta t}$, $A_5 = -1/\left(x_{\mathrm{e}} - x_{\mathrm{w}}\right)$,

$A_6 = -1/\left(y_{\mathrm{n}} - y_{\mathrm{s}}\right)$, $A_7 = -1/\left(x_{\mathrm{P}} - x_{\mathrm{W}}\right)$, $A_8 = 1/\left(x_{\mathrm{E}} - x_{\mathrm{P}}\right)$, $A_9 = -1/\left(y_{\mathrm{p}} - y_{\mathrm{S}}\right)$, $A_{10} = 1/\left(y_{\mathrm{N}} - y_{\mathrm{P}}\right)$.

The matrix is inversed analytically, so that required corrections are easily computed and are

immediately added to the values of the current solution. Under-relaxation is implemented by adding a fraction of the calculated correction to the current variables.

The cell-wise implementation described above is known to have poor convergence characteristics when grids are stretched or the flow is largely unidirectional. An improvement can be achieved by an update of variables for the entire line (column or row). This concept was firstly proposed by Zeng and Wesseling [1] who used a block-tridiagonal structure of the matrix assembled from the matrices corresponding to single lines of finite volumes. The corresponding linear equations system is solved by the standard backward-forward substitution. Our study extends the approach of [1] by derivation of an analytical solution for the system of correction equations corresponding to one line. A schematic of the developed algorithm for the two-dimensional geometry is shown in Fig.5.

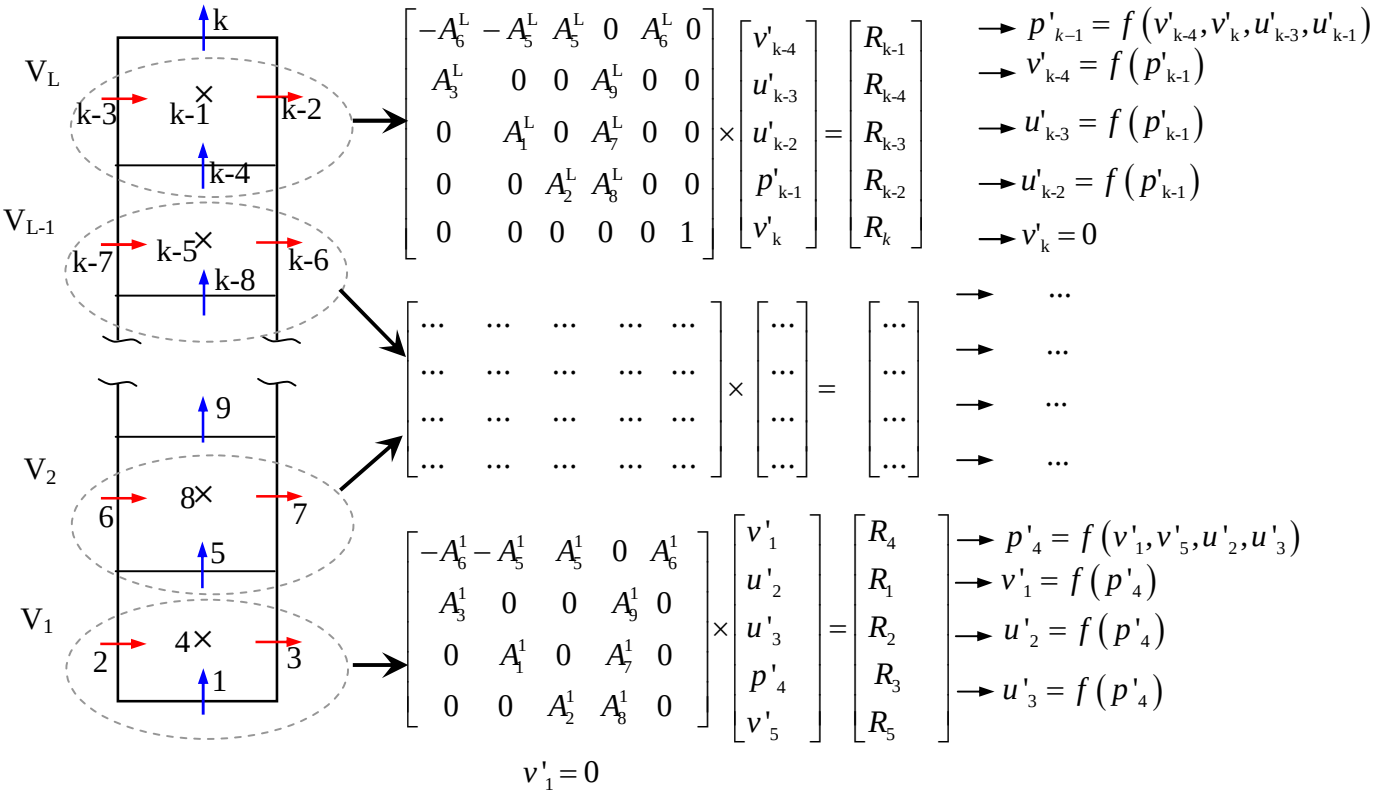

Fig.5 A schematic description of ASA-CLGS smoother.

For a 2D problem a typical column (row) consists of L finite volumes denoted by V_1 up to V_L. Each volume contains 5 unknown corrections (4 for velocity components and 1 for pressure). In total, the entire column contains k unknown corrections (see Fig. 5). Imposing Dirichlet boundary conditions for velocities, the v'_1 and v'_k are set to be equal to zero. At the next step we rearrange the characteristic matrix of Vanka's smoother [67] (see Fig.4). Starting with V_L volume (see Fig.5) the correction equation for *k-1* node is written first, and followed by the correction equations for *k-4*, *k-3*, *k-2* nodes as marked by a dotted line. Then the corrections u'_{k-2}, u'_{k-3} v'_{k-4} are written as functions of the pressure correction p'_{k-1}. Its further substitution into the correction equation for

k-1, together with a zero value of v'_{k} yields an analytical solution for the p'_{k-1}. Once the p'_{k-1} correction is found its backward substitution into the equations for *k-4*, *k-3*, *k-2* nodes yields the u'_{k-2}, u'_{k-3} v'_{k-4} corrections. The procedure is successively repeated for all volumes along the given line, providing the values of all corrections. The developed solver is easily extended to three-dimensional geometry by treating a line of three-dimensional finite volumes.

To estimate the complexity of the developed algorithm for the two-dimensional geometry we write it in a vector form as follows:

$$p'_{k-1} = \left(c_1 R_{k-2} + c_2 R_{k-3} + c_3 R_{k-4} + R_{k-1} + c_4 v'_{k}\right) / c_5$$
$$\begin{bmatrix} v'_{k-4} \\ u'_{k-3} \\ u'_{k-2} \end{bmatrix} = \begin{bmatrix} c_6 \\ c_7 \\ c_8 \end{bmatrix} \times p'_{k-1} + \begin{bmatrix} c_9 R_{k-4} \\ c_{10} R_{k-3} \\ c_{11} R_{k-2} \end{bmatrix} \qquad (20)$$

Were c_1: c_{11} are known coefficients, which are calculated only once at the beginning of the process. Thus, we need 11 multiplications and divisions and 8 summations to calculate 4 corrections (N=4) for the one volume that is approximately equal to $O(5N)$ complexity. For the three-dimensional geometry the complexity is obtained by the same way and it also does not exceed $O(5N)$ value.

5. Preliminary Results

An extensive validation study was performed with both FPCD and multigrid algorithms for two- and three-dimensional geometries. Our two-dimensional results and comparison with the previous benchmark studies [5,68,21,34] are presented in **Appendix D**[70]. It should be noted that the FPCD algorithm is extremely memory demanding for three-dimensional calculations, and as for now is restricted only to 40^3 grid resolution, which is insufficient for obtaining quantitatively reliable results [34]. This chapter presents only the multigrid algorithm validation results obtained for the three-dimensional geometry and 103^3 grid resolution.

5.1 Differentially heated cubic cavity.

Table 1 presents the comparison between the independent solutions of the present study and the benchmark solutions obtained by Wakashima and Saitoh [16] for differentially heated cavity with adiabatic horizontal walls and 120^3 grid resolution. Here the Rayleigh number Ra is equal to

$$\mathrm{Ra}=\mathrm{Gr}\times\mathrm{Pr} \qquad (21)$$

and an average Nusselt number determining the thermal flow rate trough the plane with a normal in *y* direction is :

$$\mathrm{Nu}_y = \int_0^1 \int_0^1 \left[\mathrm{Pr}\sqrt{\mathrm{Gr}} V\theta - \frac{\partial \theta}{\partial Y} \right] dx\, dz \qquad (22)$$

The obtained results are in very good agreement with the corresponding benchmark solutions reported in [16]. Note that the maximum deviation between the results does not exceed 1.3 percents. Equal Nu_y numbers obtained for both isothermal vertical boundaries validate the heat balance inside the cavity.

	Ra=10^4			Ra=10^5			Ra=10^6		
	[16]	Present	Dev .(%)	[16]	Present.	Dev (%)	16]	Present	Dev (%)
u_y max(z) (x=0.5,y=0.5)	0.1984 (0.825)	0.197 (0.825)	**0.7**	0.1416 (0.85)	0.1434 (0.85)	**1.26**	0.0811 (0.8603)	0.0802 (0.8605)	**1.1**
u_z max(x) (x=0.5,y=0.5)	0.2216 (0.177)	0.2202 (0.12)	**0.6**	0.2464	(0.068) 0.2464	**0**	0.2583 (0.0323)	0.2575 (0.0337)	**0.3**
Nu_{hot}	2.0624	2.0547	**0.37**	4.3665	4.3349	**0.72**	8.6973	8.7584	**0.05**
Nu_{cold}	--------	2.0547	-----	-------	4.3349	-----	---------	8.7584	-----

Table 1. Summary of the present and the benchmark solutions for the differentially heated cavity with adiabatic horizontal walls.

5.2 Lid-driven cubic cavity.

Figure 6 shows a comparison between velocity and pressure fields obtained by Albensoeder and Kuhlmann [55] for the cubic cavity with 96^3 grid resolution and the corresponding results of the present study. It is seen that a very good agreement exists between the velocity distributions (see Fig. 6-a) along the whole centerline for both regular and stretched grids. Regarding the pressure distribution (see Fig. 6-b), the stretched grid seems to provide more accurate results at the vicinity of the cavity boundaries and does not improve pressure field accuracy far from them.

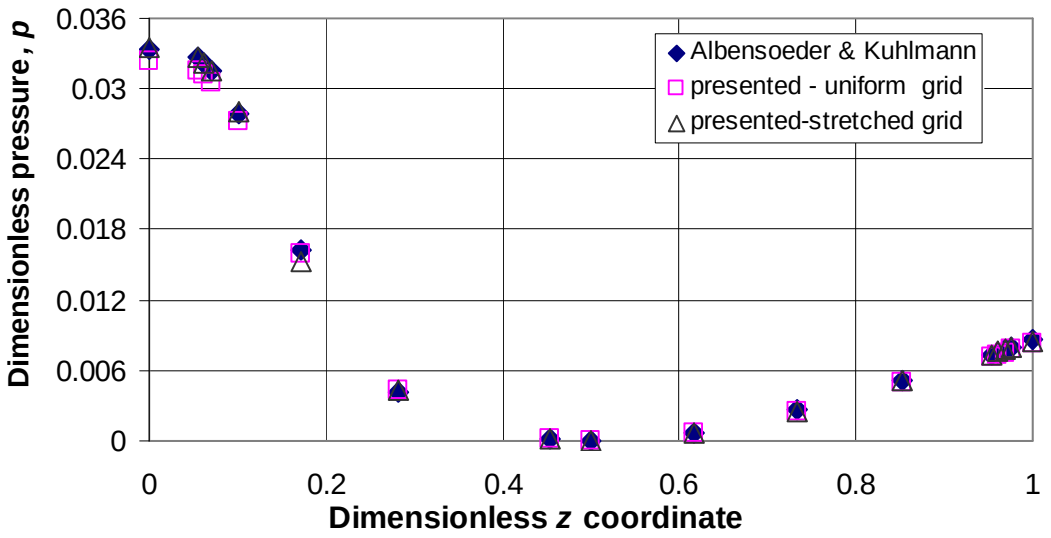

(a)

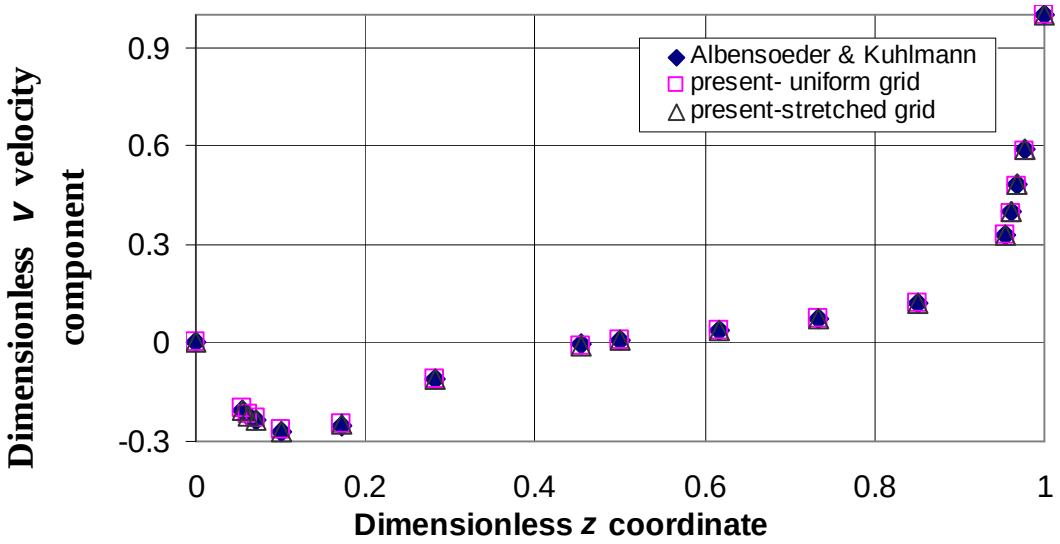

(b)

Figure 6. A comparison between Albensoeder and Kuhlman [55] and the present solutions for: (a) velocity distribution along centerline in *z* direction (*x*=0.5,*y*=0.5); (b) pressure distribution along centerline in *z* direction (*x*=0.5,*y*=0.5) .

6. Time Schedule for the Research

The detailed time schedule of the future research is detailed in table 2.

Time schedule / Planned activity	2008		2009			2010		
	6-9	10-12	1-4	5-8	9-12	1-3	4-6	7-8
Code parallelization and validation	X	X						
Semi-implicit representation of the convective terms		X	X					
Time marching numerical simulations		X	X	X	X			
Statistical post-processing				X	X	X		
Steady solver development (optional)					X	X	X	
Stability analysis (optional)						X	X	
Final Ph.D. thesis writing						X	X	X

Table 2. Time schedule for the research

The final report is expected to be ready at the second half of 2010.

7. References

1. Acharya S, Baliga BR, Karki K, Murthy JY, Prakash C, Vanka SP. Pressure-based finite-volume methods in computational fluid dynamics. *J. Heat Transfer* 2007;**129**:407-424.
2. Zeng S, Wesseling P. Numerical study of a multigrid method with four smoothing methods for the incompressible Navier-Stokes equations in general coordinates, in Melson ND, Montueffel TA, and McCormick SF (eds.), *Sixth Copper Mountain Conference on Multigrid Methods*, NASA Conference Publication 3224, 1993;691-708.
3. Trottenberg U, Oosterlee C, Schüller A. *Multigrid*, Academic Press, London, 2001.
4. De Vahl Davis G, Jones IP. Natural convection of air in square cavity: a benchmark numerical solution. *Int. J. Numer Meth. Fluids* 1983; **3**(3):249-264.
5. Le Quere P, and De Roquefort A. Computation of natural convection in two-dimensional cavities with Chebyshev polynomials. *J. Comput. Phys.* 1984; **57**:210-228.
6. Le Quere P. Accurate solutions to the square thermally-driven cavity at high Rayleigh number. *Computers & Fluids* 1991; **20**:29-410.
7. Kondo N. Numerical simulation of unsteady natural convection in a square cavity by the third-order upwind finite element method. *CFD Journal* 1994; **3**:281-302.
8. Mayne DA, Usmani A, and Crapper M. h-adaptive finite element solution of high Rayleigh number thermally-driven cavity problem. *Intl J. Numer. Heat & Fluid Flow* 2000; **10**:598-615.
9. Chan AMC, Banerjee S. 3-dimensional numerical analysis of transient natural convection in rectangular enclosures. *J.Heat Transf.* 1979;**101**:114-119.
10. Pepper DW. Modeling of three-dimensional natural convection with a time-split finite-element technique. *Numer. Heat Transf.* 1987; **11**:31-55.
11. Fusegi T, Hyun JM, Kuwahara K. Three-dimensional simulations of natural convection in a sidewall-heated cube. *Intl J. Num. Meth. Fluids* 1991; **13**:857-867.
12. Fusegi T, Hyun JM, Kuwahara K, and Fabrouk B. A numerical study of three-dimensional natural convection in a differentially heated cubical enclosure. *J. Heat Mass Transf.* 1991; **34**:1543-1557.
13. Fussegi T, Hyun JM, and Kuwahara K. A numerical study of 3D natural convection in a cube: effects of the horizontal thermal boundary conditions. *Fluid Dynam. Res.* 1991; **8**:221-230.
14. Hiller WJ, Koch ST, Kowalewski TA, Stella F. Onset of natural convection in a cube. *Intl J. Heat Mass Transf.* 1993; **36**:3251-3263.
15. Tric E, Labrosse G, Betrouni M. A first incrussion into the 3D structure of natural convection of air in a differentially heated cubic cavity, from accurate solutions. *Intl J. Heat Mass Transf.* 2000; **43**:4043-4056.
16. Wakashima S, Saitoh TS. Benchmark solutions for natural convection in a cubic cavity using the high-order time-space method. *Intl J. Heat Mass Transf.* 2004; **47**:853-864.
17. Winters KH. Hopf bifurcation in the double-glazing problem with conducting boundaries. *J. Heat Transfer* 1987; **109**:894-898.

18. Jones DN, Briggs DG. Periodic Two-Dimensional Cavity Flow: Effect of Linear Horizontal Thermal Boundary Condition. *J. Heat Transfer* 1989; **111**:86-91.
19. Le Quere P, and Behnia M. From onset of unsteadiness to chaos in a differentially heated square cavity. *J. Fluid Mech.* 1998; **359**:81-107.
20. Le Quere P. Transition to unsteadiness routes to chaos and simulation of turbulent flows in cavities heated from the side: a review of present status. In *Heat transfer*: *Proceedings of the 10th Intl Heat transfer Conf.* 1994; **1**:281-296.
21. Xin S. and Le Quere P. An extended Chebyshev pseudo-spectral benchmark for the 8:1 differentially heated cavity. *Intl J. Num. Meth. Fluids* 2002*;* **40**:981-998.
22. Christon MA, Gresho PM, and Sutton SB. Computational predictability of time-dependent natural convection flows in enclosures (including a benchmark solution) *Intl J. Numer. Meth. Fluids* 2002; **201**: 953-980.
23. Tian YS, Karayiannis TG. Low turbulence natural convection in an air filled square cavity Part I: the thermal and fluid flow fields. *Intl J. Heat Mass Transf.* 2000; **43**:849-866.
24. Tian YS, Karayiannis TG. Low turbulence natural convection in an air filled square cavity Part I: the thermal and fluid flow fields. *Intl J. Heat Mass Transf.* 2000; **43**:8866-8884.
25. Salat J, Xin S, Joubert P, Sergent A, Penot F, Le Quere P. Experimental and numerical investigation of turbulent natural convection in a large air-filled cavity. *Intl J. Heat. Fluid Flow* 2004; **25**:824-832.
26. Jansen RJA, Henkes RAWM, and Hoogendoorn CJ. Transition to time-periodicity of a natural-convection flow in a 3-D differentially heated cavity. *Intl J. Heat Mass Transfer* 1993; **36**(11): 2927-2940.
27. Jansen RJA, Henkes RAWM. Instabilities in three-dimensional differentially-heated cavities with adiabatic horizontal walls. *Phys. Fluids* 1996; **8**(1):62-74.
28. Fusegi T, Hyun J, and Kuwahara K. Three-dimensional numerical simulation of periodic natural convection in differentially heated cubical enclosure. *Appl. Sci. Res*. 1992; **49**: 271-282.
29. Labrosse G, Tric E, Khallouf H, and Betrouni M. A direct (pseudo-spectral) solver of the 2-D/3-D Stokes problem: transition to unsteadiness of natural-convection flow in a differentially hated cubical cavity. *Numer Heat Transfer B* 1997; **31**:261-276.
30. Soria M, Trias FX, Perez-Segarra CD, Oliva A. Direct numerical simulation of a three-dimensional natural-convection flow in a differentially heated cavity of aspect ratio 4. *Num. Heat Transfer, Part A* 2004; **45**: 649-673.
31. Trias FX, Soria M, Oliva A, and Perez-Segarra CD. Direct numerical simulations of two-and three-dimensional turbulent natural convection flows in a differentially heated cavity of aspect ratio 4. *J. Fluid Mech*. 2007 **586**:259-293.
32. Versteegh TAM, Nieuwstadt FTM. A direct numerical simulation of natural convection between two infinite vertical differentially heated walls scaling laws and wall functions. *Intl J. Heat Mass Transf.* 1999; **42**:3673-3693.

33. Aounallah M, Addad Y, Benhamadouche S, Imine O, Adjlout L, Laurence D. Numerical investigation of turbulent natural convection in an inclined square cavity with a hot wavy wall. *Intl J. Heat Mass Transf.* 2007; **50:**1683-1693.
34. Gelfgat AYu. Stability of convective flows in cavities: Solution of benchmark problems by low-order finite volume method. *Intl J. Num. Meth. Fluids* 2006; **53**:485-506.
35. Ghia U, Ghia KN, Shin CT. High-Re solutions for incompressible flow using Navier-Stokes equations and a multigrid method. *J. Comput. Phys*. 1982; **48**:387-411.
36. Shreiber R, Keller HB. Driven cavity flows by efficient numerical techniques. *J. Comput. Phys.* 1983; **49**:310-333.
37. Burggraf OR. Analytical and numerical studies of the structure of steady separated flows. *J. Fluid Mech.* 1966; **24**:113-151.
38. Pan F, Acrivos A. Steady flows in rectangular cavities. *J. Fluid Mech.* 1967; **28**:643-655.
39. Koseff JR, Street RL, Gresho PM, Upson CD, Humphrey JAC, To WM. A three-dimensional lid-driven cavity flow: experiment and simulation, in: *Proceedings of 3rd International Conference on Numerical Methods in Laminar and Turbulent Flow* 1983; 564-581.
40. Freitas CJ, Street RL, Findikakis AN, Koseff JR. Numerical simulation of three-dimensional flow in a cavity. *Intl J. Numer. Meth. Fluids* 1985; **5**:561-575.
41. Botella O, Peyret R. Benchmark spectral results on the lid-driven cavity flow. *Comput. Fluids* 1998; **27**:421-433.
42. Gelfgat AYu. Implementation of arbitrary inner product in the global Galerkin method for incompressible Navier-Stokes equations. *J. Comput. Phys*. 2006; **211**:513-530.
43. Davis GDe, Mallinson GD. An evaluation of upwind and central difference approximations by a study of recirculating flow. *Comp. Fluids* 1976; **4**:29-43.
44. Goda K, A multistep technique with implicit difference schemes for calculating two- or three-dimensional cavity flows. *J. Comput. Phys*. 1979; **30**:76-95.
45. Freitas CJ, Street RL, Findikakis AN, Koseff JR. Numerical simulation of three-dimensional flow in cavity. *Intl J. Numer. Meth. Fluids* 1985; **5**:561-575.
46. Koseff JR, Street RL. On end wall effects in alid-driven cavity flow. *J. Fluids Eng*. 1984; **106**:385-389.
47. Ku HC, Hirsh RS,Taylor TD. A pseudospectral method for solution of the three-dimensional incompressible Navier-Stokes equations. *J. Comput. Phys*. 1987; **70**:439-462.
48. Cortes AB, Miller JD. Numerical experiments with the lid-driven cavity flow problem. *Comput. Fluids* 1994; **23**:1005-1027.
49. Babu V, Korpela SA. Numerical solutions for incompressible, three-dimensional Navier-Styokes equations. *Comput. Fluids* 1994; **23**:675-691.
50. Wang MMT, Sheu TWH. An element-by-element BICGSTAB iterative method for three-dimensional steady Navier-Stokes equations. *J. Comp. Appl. Math.* 1997; **79**: 147-165.
51. Iwatsu R, Ishii K, Kuwahara K, Hyun JM. Numerical simulation of three dimensional flow structure in a driven cavity. *Fluid Dyn. Res*. 1989; **5**:173-189.

52. Chiang TP, Sheu WH, Hwang RR. Three-dimensional vortex dynamics in a shear-driven rectangular cavity. *Intl J. Comput. Fluid Dyn*. 1997; **8**:201-214.
53. Chiang TP, Sheu WH, Hwang RR. Effect of Reynolds number on the eddy structure in a lid-driven cavity. *Intl J. Num. Meth. Fluids* 1998; **26**:557-579.
54. Sheu TWH, Tsai SF. Flow topology in a steady three-dimensional lid-driven cavity. *Comput. Fluids* 2002; **31**:911-934.
55. Albensoeder S, Kuhlmann HC. Accurate three-dimensional lid-driven cavity flow. *J. Comput. Phys.* 2005; **206**:536-558.
56. Goodrich JW, Gustafson K, Halasi K. Hopf bifurcation in the driven cavity. *J. Comput. Phys.* 1990; **90**:219-261.
57. Shen J. Hopf bifurcation of the unsteady regularized driven cavity flow. *J. Comput. Phys.* 1991; **95**:228-245.
58. Auteri F, Parolini N, Quartapelle L. Numerical investigation on the stability of singular driven cavity flow. *J. Comput. Phys.* 2002; **183**:1-25.
59. Auteri F, Quartapelle L,Vigevano L. Accurate $\omega-\psi$ spectral solution of the singular driven cavity flow. *J. Comput. Phys.* 2002; **180**:597-615.
60. Abouhamza A, Pierre R. A neutral stability curve for incompressible flows in a rectangular driven cavity. *Math. Comput. Model*. 2003; **38**:141-157.
61. Albensoeder S, Kuhlmann HC, Rath HJ. Three-dimensional centrifugal-flow instabilities in the lid-driven cavity problem. *Phys. Fluids* 2001; **13**:121-135.
62. Deville M, Lê TH, Y. Morchisne. Numerical simulation of 3-D incompressible unsteady viscous laminar flows. *Notes on Numer. Fluid Mech.* 1992; **36**.
63. Leriche E, Gavrilakis S. Direct numerical simulation of the flow in a lid-driven cubical cavity. *Phys. Fluids* 2000; **12**:1363-1376.
64. Bouffanais R, Deville MO, Fisher PF, Leriche E, Weill D. Large-eddy simulation of the lid-driven cubic cavity flow by the spectral element method. *J. Scientif. Comp*. 2006; **27**:151-161.
65. Patankar SV. *Numerical Heat Transfer and Fluid Flow*, McGraw-Hill, New York, 1980.
66. van der Vorst HA. *Iterative Krylov methods for large linear systems*, Cambridge Unversity Press, 2003.
67. Vanka SP. Block-implicit multigrid solution of Navier-Stokes equations in primitive variables. *J. Comput. Phys.*1986; **65**: 138-158.
68. Vanka SP. A Calculation Procedure for three-dimensional steady recirculating flows using multigrid methods. *Comp. Meth. Applied Mechan. Enginer.*1986; **55**: 321-338.
69. Brandt A. Multi-level adaptive solutions to boundary-value problems. *Mathem. of Computation* 1977; **31**(138):333-390.
70. http://www.eng.tau.ac.il/~gelfgat/Feldman_WWW/Feldman_Contents.htm